Acceptor states in the photoluminescence spectra of *n*-InN

A. A. Klochikhin
A.F. Ioffe Physico-Technical Institute 194021, St. Petersburg, Russia
and Petersburg Nuclear Physics Institute 188350, St. Petersburg, Russia

V. Yu. Davydov, V. V. Emtsev, A. V. Sakharov, and V. A. Kapitonov
A.F. Ioffe Physico-Technical Institute 194021, St. Petersburg, Russia

B. A. Andreev
Institute for Physics of Microstructures RAS, GSP-105, 603950 Nizhny Novgorod, Russia

Hai Lu and William J. Schaff
Department of Electrical and Computer Engineering, Cornell University, Ithaca, New York 14853, USA
(Received 15 December 2004; published 26 May 2005)

Interband photoluminescence (PL) and absorption spectra of *n*-InN samples with Hall concentrations from 3.6×10^{17} to 6×10^{18} cm^{-3} were studied. Sample thicknesses were in the range from 12 to 0.47 μm. A set of lasers for the PL excitation in the energy range from 2.41 down to 0.81 eV was used. The well-resolved structure consisting of three peaks was observed in the PL spectra of the high-quality samples in the energy interval from 0.50 to 0.67 eV at liquid-helium and nitrogen temperatures. We attributed one of two low-energy features of the spectra to the recombination of degenerate electrons with the holes trapped by deep acceptors with a binding energy of $E_{da}=0.050-0.055$ eV, and the other one was attributed to the LO-phonon replica of this band. The higher-energy PL peak is considered as a complex band formed by two mechanisms. The first one is related to the transitions of electrons to the states of shallow acceptors with a binding energy of $E_{sh}=0.005-0.010$ eV and/or to the states of the Urbach tail populated by photoholes. The second mechanism contributing to this band is the band-to-band recombination of free holes and electrons. The relative intensities of the two higher-energy PL peaks were found to be strongly dependent on temperature and excitation power. A model approach taking into account the Urbach tails of conduction and valence bands and the acceptor states was developed. The calculations of PL and the absorption spectra have shown that the band gap of InN in the limit of zero temperature and zero electron concentration is close to 0.665–0.670 eV. The model calculations allowed us to explain the structures of all the spectra observed, their dependence on the excitation power, and the temperature variations of PL and the absorption spectra. The effective masses of electrons at the Γ point equal to 0.042 and 0.07 of free-electron mass were tested in calculations. The conductivity band was assumed to be nonparabolic.

DOI: 10.1103/PhysRevB.71.195207 PACS number(s): 78.55.Cr, 78.20.Bh, 78.66.Fd, 71.55.Eq

I. INTRODUCTION

It is known that the spectra of interband photoluminescence (PL) of nondegenerate direct-gap semiconductors are strongly influenced by excitons or electrons and holes localized at impurities, because the energy relaxation time of photoexcited carriers is typically much shorter than the radiative lifetime, and, hence, the carriers or excitons populate the localized states before radiative annihilation. As a consequence, the PL spectra exhibit the structure due to localized states.

At the early stages of studies,[1,2] the InN materials had very high electron concentrations $n_e\sim10^{20}-10^{21}$ cm^{-3}, and no photoluminescence was observed. For this reason, the band gap of this material could be estimated in absorption measurements alone. Later it was found that the infrared luminescence of InN was observable in samples having electron concentrations of $n_e\approx1-2\times10^{19}$ cm^{-3} and less.[3–6]

The heavily doped degenerate semiconductors, such as the *n*-type InN crystals with an electron concentration well above 10^{18} cm^{-3}, are characterized by band-to-band photoluminescence.[3–9] The PL bands are structureless because of the screening of the Coulomb interaction followed by the disappearance of excitons, shallow donor and acceptor states, and their complexes. The interband absorption threshold of such materials is shifted towards higher energies due to the band-filling Burstein-Moss effect[10] and can exceed considerably the band gap of InN.

Very recently, thick *n*-InN films with charge carrier concentrations below 4×10^{17} cm^{-3} and room-temperature Hall mobilities higher than 2100 cm^2/V s were produced.[11,12] At present, a good deal of experimental information concerning high-quality *n*-InN samples has been reported in the literature (Refs. 13–18 and references therein).

The PL studies of degenerate samples of *n*-InN with relatively low electron concentrations of the order of $n_e\approx\times10^{18}$ cm^{-3} revealed that the exponentially decreasing density-of-states tails of the valence and conduction bands, formed by shallow localized electrons and holes, can manifest themselves in the formation of the PL band. The band gap was estimated to be about 0.670 eV, even

though these Urbach tails lead to some uncertainty in this value.[19]

The theoretical calculations of the band structure of InN (Refs. 20–23) have shown that the band gap of this semiconductor is narrow, consistent with the experimental data. The dielectric function of InN films was studied by spectroscopic ellipsometry in Refs. 24–26, and the energy positions of the van Hove singularities were established in a wide energy range.

Wu *et al.*[13] used the optical absorption technique to measure the temperature dependence of the fundamental band gap of InN grown by molecular beam epitaxy (MBE). For 7.5-μm-thick layers with Hall concentrations of 4×10^{17} cm^{-3}, the fundamental band gap was estimated to be 0.690 eV. The position of the PL band was assumed to be affected by emission from localized states. The band-gap variation with temperature over an interval of 4.2 K to 295 K was estimated to be 49 meV. As follows from the data presented in Ref. 13, the PL-band maximum shifts by 30 meV to lower energies within the temperature interval given above, i.e., it is less than the band-gap shrinkage.

In the present paper it will be shown that a considerable difference between the band-edge shrinkage and the temperature-dependent shift of the PL-band maximum, mentioned in Ref. 13 and often reported by other authors, is inherent in the band-to-band recombination when the free hole states are involved in the process. Therefore, the temperature behavior of the PL band clarifies the PL formation mechanism.

Chen *et al.*[15–17] have conducted subpicosecond-resolution-differential transmission measurements on InN epilayers to study the carrier recombination dynamics and hot carrier relaxation processes in these materials at room temperature. The authors[15] concluded that at short time delays after pulsed excitation the longitudinal optical-phonon scattering is a dominant energy-relaxation process. At longer delays, a redshift of the peak energy in the differential transmission spectra was recorded. This redshift was explained as a result of the reduced band-filling effect when the photoexcited carriers recombine. Temperature-dependent PL measurements[16] have confirmed that in the high-quality samples with electron concentrations of (4×10^{17} cm^{-3}) the peak redshift is nearly in the same energy interval as that reported in Ref. 13. A linear dependence of the charge-carrier lifetime on the charge-carrier concentration[17] was observed in the concentration range from 4×10^{17} to 1.2×10^{19} cm^{-3}.

We will demonstrate in this paper that the steady-state luminescence also provides evidence of a fast rate of the relaxation process, resulting in an equilibrium or almost equilibrium distribution of photoholes over their energies before annihilation. In addition, the electron-phonon interaction with the optical modes will be shown to lead to the complicated PL spectra of interband transitions.

Arnaudov *et al.*[18] have investigated the low-temperature PL spectra for 0.2- to 1.5-μm-thick epitaxial *n*-InN layers with Hall concentrations in the range from 7.7×10^{17} to 6×10^{18} cm^{-3}. They have proposed three different concentration-dependent mechanisms of the PL formation. The PL spectra at a moderate doping level are interpreted as the recombination of free degenerate electrons with holes bound by the acceptors. For heavily doped samples with charge-carrier concentrations above 5×10^{18} cm^{-3}, the recombination of nonequilibrium free holes is put forward to describe the PL. In turn, the PL bands at 673 and 605 meV of samples with a low doping level are attributed to the recombination of nondegenerate electrons from the bottom of the conduction band at two states of shallow and deep acceptors, respectively. The value $E_g=0.692$ eV was obtained in Ref. 18 as a result of the best fit of the experimental spectra at the electron effective mass at the Γ point equal to $m_e=0.042$ of the free electron mass.

It should also be mentioned that up to now conflicting opinions about the fundamental parameters of InN can be found in the literature. Among the parameters of practical importance for the understanding of optical experiments, the band-gap value, the electron effective mass, and the probable nonparabolicity of the conduction band in InN, connected with the problem of common-cation-rule breaking, are the hot issues under discussion.

Wu *et al.*[7] have studied the infrared reflection from wurtzite InN layers within a range of the free-electron concentrations typical of samples grown by molecular beam epitaxy. Measurements of the plasma-edge frequencies were used to determine the electron effective mass. The results revealed a pronounced increase in the electron effective mass with increasing electron concentration, thus providing evidence of the nonparabolic conduction band in InN.

Inushima, Higashiwaki, and Matsui[9] have studied the optical properties of Si-doped InN. The charge-carrier concentration was varied from 1.8×10^{18} to 1.5×10^{19} cm^{-3}. The effective mass also showed a rise as the electron concentration increased, and at $n_e=8\times10^{18}$ cm^{-3} its value was around $0.085m_0$.

Carrier and Wei[27] have found in their calculations a strong nonparabolicity of the conductivity band and a linear dependence of the effective mass of an electron on its kinetic energy. The electron effective mass at the Γ point was estimated to be $0.07m_0$. It has been shown that the nonparabolicity has a strong effect on the interband-absorption coefficient over a wide energy interval.

We will show in this paper that the problem of the electron effective mass is closely related to other questions, such as a marked disparity between charge-carrier concentrations estimated from optical and electrical data.

As pointed out in Ref. 5, the PL-band shape as well as the absorption-coefficient behavior are strongly affected by the inhomogeneous spatial distributions of the electron density of which the origin is not clear. Recent results [28–32] have conclusively shown that considerable inhomogeneity in the growth direction is typical of the epitaxial InN layers.

An intrinsic surface-electron accumulation layer in the *n*-InN samples was revealed by Lu *et al.*,[28] who studied transport characteristics of very thin InN films, down to 10 nm in thickness, with charge-carrier concentrations of the order of 10^{18} cm^{-3}. A strong excess sheet charge was detected. This charge stems from either the surface or the interface between the InN and its buffer layer. The

capacitance-voltage measurements have shown that the charge carrier concentration ranges from 10^{20} to 10^{18} cm^{-3} at a depth of 6 nm from the InN surface.[28]

The experimental studies of the conduction-band electron plasma performed by Mahboob *et al.*[29] revealed that donor-type surface states can exist in the conduction band. These surface states become ionized by emitting their electrons into the conduction band. They manifest themselves as a surface-electron-accumulation layer that is required to neutralize the positively charged surface states.

New variable magnetic-field Hall-effect measurements were conducted by Swartz *et al.*[32] on InN samples grown by molecular-beam epitaxy. As distinct from ordinary Hall-effect measurements producing only averaged data for inhomogeneous materials, the above-mentioned technique allows direct measurements of interfacial and/or surface conductivity and the electrical properties of the bulk. These measurements revealed the charge-carrier groups with different mobilities. This suggests the presence of multiple conduction layers as well as sample inhomogeneity. The quantitative technique for the mobility-spectrum analysis reported in Ref. 32 also points to a continuous and considerable spread in mobility for the electrons in bulk InN, in much the same way as is observed in layers of various thicknesses. The analysis of a 7.5-μm-thick InN sample has shown that the maximum mobility of electrons exceeds 3500 $cm^2/V\,s$ for "bulk" InN.

The main purpose of the present paper is to analyze the optical data obtained on *n*-InN samples of high quality, together with some new data gained by other investigators for similar materials. The approach suggested in this paper is aimed at minimizing the uncertainties in the basic parameters of InN that are still existing in the literature.

The paper is organized as follows. Section II outlines the experimental setup and sample characterization. Sec. III is devoted to the model used for the description of optical data. In Sec. IV the results of the model calculations are given and discussed. The most important findings are summarized in Sec. V.

II. EXPERIMENTAL DATA

A. Experimental setup

Photoluminescence (PL) measurements were performed by pumping with an Ar^+-ion laser operating at 2.41 eV (514.5 nm). The pump power density was varied between 10 mW/cm^2 and 1 W/cm^2. The InN samples were mounted in a liquid-helium cryostat and cooled to a temperature of about 4.2 K. The luminescence signal was analyzed by a BOMEM DA3.002 high-resolution Fourier spectrometer and detected with a liquid-nitrogen-cooled InSb detector (cutoff energy $\approx$0.4 eV, $\lambda \approx 3.1$ μm) with a resolution 4 cm^{-1}. The PL spectra of the InN samples were corrected by using the emission spectrum of a tungsten lamp.

Additionally, the PL spectra were measured at liquid-nitrogen temperature (77 K) by using as excitation sources a frequency-doubled solid-state YAG:Nd (where YAG is ytrium aluminum garnet) laser with 2.33 eV ($\lambda = 532$ nm) or different semiconductor lasers with 0.81–1.55 eV (1550–800 nm). An uncooled InGaAs PIN diode was used as a detector (cutoff energy$\approx$0.59 eV, $\lambda \approx 2.1$ μm). The maximum excitation power densities were $\approx$0.3 kW/cm^2 and $\approx$50 W/cm^2 for the solid-state and semiconductor lasers, respectively. The excitation densities were varied by neutral density filters (for the solid-state laser) or by changing the injection current (for the semiconductor lasers).

B. Characterization of samples

InN films were grown on (0001) sapphire substrates by different techniques in three different laboratories. The major part of the samples studied was grown by the MBE technique at Cornell University (USA). Typically, an AlN nucleation layer and a GaN buffer layer were deposited prior to InN growth.[11] The InN-layer thicknesses of the samples used in our studies ranged from 470 nm to 12 μm. Although the samples were not intentionally doped, free-electron concentrations ranging from 3.6×10^{17} to 8.4×10^{17} cm^{-3} were found in the samples by Hall-effect measurements.

In addition, two nonintentionally doped InN samples E233-5 and 000702 grown by the molecular beam epitaxy (MBE) and metalorganic vapor phase epitaxy (MOVPE) techniques at Chiba and Fukui Universities (Japan), respectively, were studied. The thicknesses of the MBE- and MOVPE-grown samples were 1.7 and 0.5 μm and their electron concentrations were 2×10^{18} cm^{-3} and 8×10^{18} cm^{-3}, respectively. More details of the growth of these samples can be found in Refs. 33 and 34.

For convenience, the samples were divided into three groups. The parameters of the samples are presented in Table I.

The samples of the first group are the thick layers characterized by the Hall electron concentrations less than 10^{18} cm^{-3}. The samples of the second group are thin layers with concentrations close to 10^{18} cm^{-3}. The samples of the third group have concentrations above 10^{18} cm^{-3}.

The concentration values n_{opt} were obtained from the model fitting of the PL spectra (see Sec. IV).

C. Quantum yield of photoluminescence

A strong dependence of the quantum yield of luminescence on the sample quality was observed. To estimate the external quantum efficiency B_Q(ext) of the InN samples, the PL spectrum of the reference Si:Er/Si-MBE structure with a known B_Q(ref) was measured. The B_Q(ref) of the Si:Er/Si structure (emitting at $\lambda = 1.54$ μm) was measured by a NOVA OPHIR instrument with a PD300-IR detector (minimal detectable power was $\approx$1 nW). The value of the B_Q(ref) of the Si:Er/Si structure was 4×10^{-3} at the pump power $P_{ex}=4$ mW and $T=4.2$ K. The B_Q(ext) of the InN layers was determined as

$$B_Q(\text{ext}) \approx B_Q(\text{ref}) \times [\text{PL(InN)}/\text{PL(ref)}],$$

where PL(InN) and PL(ref) are the integrated intensities of InN and Si:Er/Si, respectively. The quantum yield of the luminescence was found to decrease by approximately a factor of 5 in the range of the Hall concentrations studied.

The quantum yields of some InN samples measured by a InSb detector at excitation powers of 100 mW at 4.2 K are given in Table I.

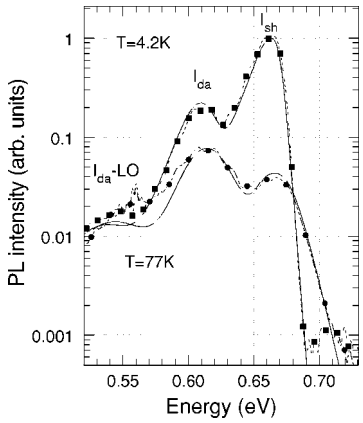

FIG. 1. PL spectra of thick sample Gs2060 at liquid helium and nitrogen temperatures (upper and lower decorated curves, respectively). The solid lines represent the results of model fits. In calculations, the maximum I_{sh} is composed of two processes: (i) the band-to-band recombination of free electrons and holes and (ii) the annihilation of free electrons and holes localized by shallow acceptors with binding energies $E_{sh} \approx 5-10$ meV. The maximum I_{da} is considered as a recombination of electrons with holes localized by deep acceptors ($E_{da} \approx 50-55$ meV, and the maximum I_{da}-LO is built as a LO-phonon replica of the previous transition.

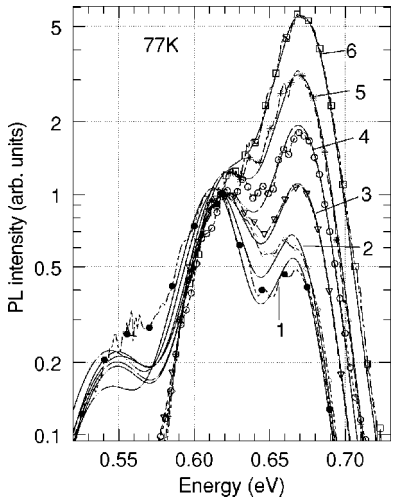

FIG. 2. Variations of the PL spectrum of sample Gs2060 with the excitation power at nitrogen temperature. The decorated curves are experimental data, and the solid lines are the results of model calculations. The PL spectrum 1 was detected by an InSb diode at the minimal excitation power, and spectra 2–6 were obtained with a InGaAs detector. Spectra 1–5 were obtained in the cw-excitation regime, and for spectrum 6 the pulsed excitation was used. The spectra are normalized at 0.61 eV. The results of the model calculations were obtained at different positions of the hole-chemical potential, assuming a quasiequilibrium distribution of photoholes and increasing electron concentrations.

D. General features of the PL and absorption spectra

The PL spectra of sample Gs2060 at liquid-helium and nitrogen temperatures measured at steady-state excitation are presented in Fig. 1. Note that spectra of all thick samples are influenced by the Bragg interference. The most striking features of the spectra are the structure consisting of three peaks and the sensitivity to the temperature variation.

The structure of the spectra of the high-quality samples can occur as a natural result of the recombination of holes trapped by the impurity centers. The energy position of the middle peak agrees well with the data of Ref. 18 and can be attributed to the annihilation of the holes localized by deep acceptor states. The lowest-energy peak of the spectra is shifted toward lower energy by the LO-phonon energy[35] and, therefore, can be regarded as a manifestation of the electron-phonon interaction. It will be shown in Secs. III and IV that both shallow localized and band states of holes should be taken into account to interpret the high-energy peak.

As can be seen in Fig. 1, the rise from liquid-helium to nitrogen temperature leads to the redistribution of intensities between the two high-energy peaks. This transformation of the spectrum with temperature may be explained in two alternative ways. The first one assumes an increase of the energy-relaxation rate of nonequilibrium holes in shallow localized and band states followed by an increasing population of deep acceptor states.

The other version assumes that saturation of the localized states by photoholes is reached, and an equilibrium or

TABLE I. Sample parameters: n_{Hall} and μ_{Hall} are carrier concentrations and mobilities, respectively, measured by the Hall effect, t are samples thicknesses, n_{opt} are carrier concentrations obtained from the fit of the optical data, assuming a nonparabolic conduction band and the effective electron mass at the Γ-point of $m_\Gamma = 0.07 m_0$, and B_Q(ext) are quantum yields.

Sample no.	n_{Hall} (cm^{-3})	μ_{Hall} ($cm^2/V\,s$)	t μm	n_{opt} (cm^{-3})	B_Q(ext) 10^{-2}
Gs2060	3.6×10^{17}	2000	12.0	2.4×10^{17}	9.0
Gs2050	5.7×10^{17}	1600	7.0	2.4×10^{17}	7.5
Gs1804	7.3×10^{17}	1300	1.7	2.4×10^{17}	9.0
Gs2055	1.0×10^{18}	1050	0.42	4.3×10^{17}	4.0
Gs2019	2.6×10^{18}	1050	0.6	8.4×10^{17}	
E233-5	2.0×10^{18}	1500	1.7	1.45×10^{18}	2.0
000702	8.0×10^{18}	500	0.5	3.45×10^{18}	

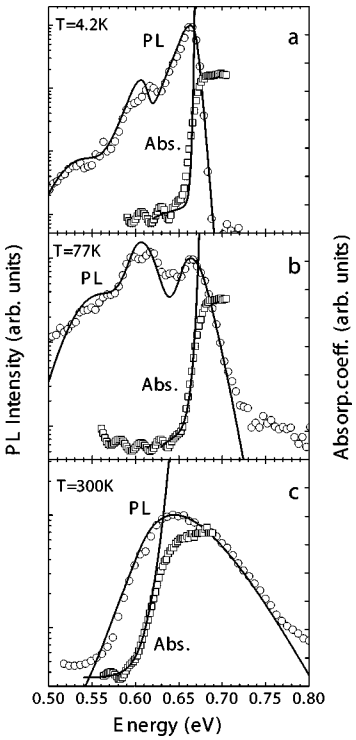

FIG. 3. Variations of the PL and absorption spectra of sample Gs2050 with a temperature increase. The symbols are the experimental data, and the solid lines are the results of model calculations. (a) $T=4.2$ K, (b) $T=77$ K, and (c) $T=300$ K.

almost-equilibrium distribution of holes is established. This version involves an increase in the nonradiative process rate with temperature followed by the shift of the photohole population border toward the band gap.

It is well known that the PL intensity decreases as temperature increases, which also points to the enhancement of the nonradiative processes and makes the second variant of the explanation preferable. On the other hand, the second version means that the concentration of the localized states that can be populated by holes is low enough, because the excitation powers, at which the redistribution was observed, were rather low.

An additional argument supporting the second version is given by the PL sensitivity to the excitation power. Figure 2 demonstrates the transformations of the PL spectrum of sample Gs2060 in a wide interval of the excitation powers at nitrogen temperature. It can be seen from Fig. 2 that spectra registered by InSb and InGaAs detectors coincide well in a wide range of energies above 0.6 eV.

At low and middle excitation densities an intensity redistribution between two high-energy peaks is observed. The further increasing of the excitation power results in a high-energy shift of the spectrum and a broadening of the high-energy peak due to the carrier concentration's increasing. A similar dependence was observed at liquid-helium temperature.

It is worth noting that the observed dependence can be understood only in the framework of the second version, as a result of the population-border shift.

Figures 3(a)–3(c) show the temperature dependences of the PL and the absorption spectra in a wide temperature interval. The most dramatic transformation of the PL spectrum occurs from nitrogen temperature to room temperature.

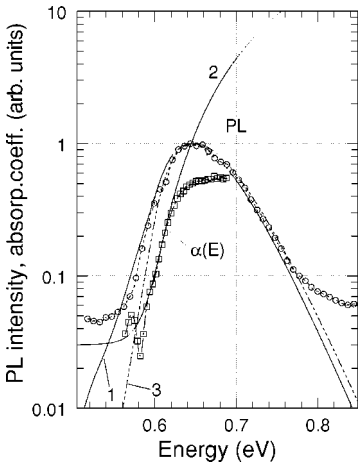

FIG. 4. Experimental PL and absorption spectra of sample Gs2050 at room temperature (symbols), and model spectra (solid lines 1 and 2). Dashed line 3 is the result of model calculations without acceptor states.

The calculations in Secs. III and IV show that these changes in the PL spectra are due to the alterations of the microscopic mechanism of the PL formation. At room temperature, the dominant role is played by the band-to-band transitions as a result of the population of the valence-band states. Figure 4 presents the details of the analysis of the room-temperature PL spectrum.

Figure 5 demonstrates a comparison of the PL spectra of samples of the first group. As can be seen in Fig. 5, the spectra have similar structures, and the only detectable difference between them is the different ratios between the intensities of the high-energy and the second maxima, which increase as the sample thickness decreases from 12 to 1.7 μm.

Figures 6–9 demonstrate the dependences of the PL spectra on temperature and on the excitation power for thin

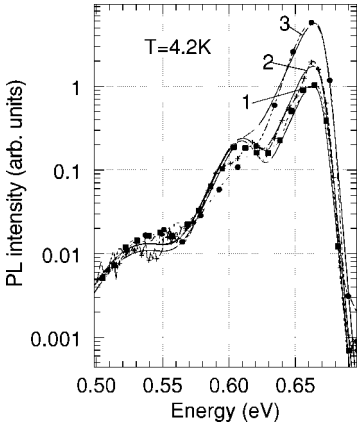

FIG. 5. PL spectra of samples Gs2060, Gs2050, and Gs1804 of the first group (curves 1, 2 and 3, respectively) at liquid-helium temperature. The symbols are experimental data, and the solid lines give results of model fits. The spectra are normalized at 0.61 eV.

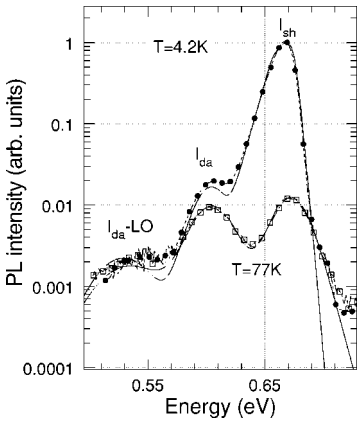

FIG. 6. PL spectra of thin sample Gs2055 of the second group at liquid-helium and nitrogen temperatures (decorated, dashed upper and lower curves, respectively). The spectra are normalized at 0.55 eV. The solid lines represent the results of model calculations.

samples of the second group. Despite the difference in the electron concentrations, the major features of the spectra of the first and second groups coincide. The explanations of the temperature and excitation-power variations of these spectra are the same.

Figure 10 shows the PL spectra of the sample of the third group with a relatively high carrier concentration. The spectra were detected at two excitation powers differing by a factor of 47. The features typical of the PL spectra of the highly doped InN can be seen, but a weak dependence on the excitation power is still conserved.

In Fig. 11, the PL spectra of samples of the second and third groups are shown and they demonstrate the shift of the PL band with carrier concentration increase.

III. THEORY

A. The density of valence-band states

The InN samples of improved quality demonstrate more intensive PL bands with exponentially decreasing tails

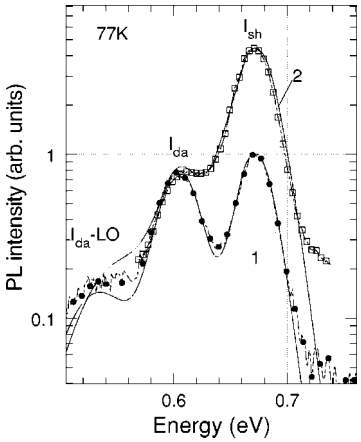

FIG. 7. PL spectra of sample Gs2055 for two excitation powers at nitrogen temperature. The spectra were normalized at high-energy maxima. The results of the model calculations (solid curves) were obtained at different positions of the hole chemical potential, assuming an equilibrium distribution of photoholes.

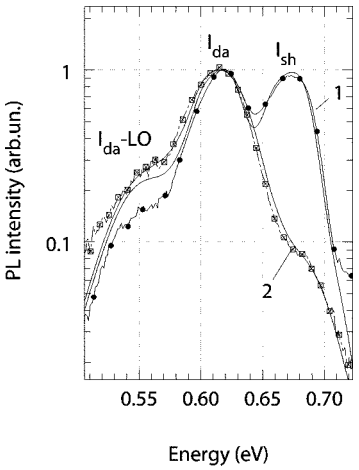

FIG. 8. PL spectra of sample Gs2019 at He (curve 1) and nitrogen (curve 2) temperatures normalized at 0.61 eV. The solid lines give the results of the model calculations. I_{sh}, I_{da}, and I_{da}-LO are maxima due to the recombination of free electrons and holes localized by shallow and deep acceptors, and the phonon replica of the band, due to deep acceptors.

formed by donor-acceptor annihilation of shallow localized electron and hole states.[19] Tails of this kind are known to appear in disordered systems, such as solid solutions and amorphous semiconductors, as a result of the random distribution of atoms over lattice sites or the structural imperfections randomly scattered over the crystal. The formation of the tails of localized states leads to significant changes in the interband absorption and the PL spectra. In the case of doped semiconductors, the spatial arrangement of doping centers plays the role of a random factor.

One can expect that, in the case of lower doping, the localized hole states of acceptor-type impurities and the tail states of the conduction band will play a noticeable role in the formation of the interband luminescence. Then additional

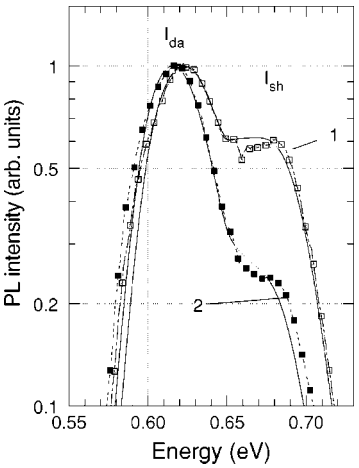

FIG. 9. PL spectra of sample Gs2019 at different excitation powers and at nitrogen temperature (decorated curves 1 and 2). The excitation power for curve 2 is decreased by a factor of 47. The spectra are normalized at 0.61 eV. I_{sh} and I_{da} are maxima due to the recombination of free electrons and holes localized by different acceptors. The solid lines are model fits.

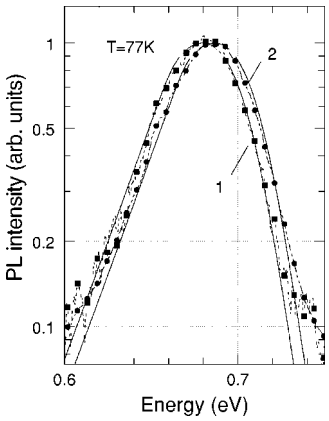

FIG. 10. PL spectra of sample E233-5 at nitrogen temperature obtained at a low excitation power (curve 1, symbols) and at an excitation power increased by a factor of 267 (curve 2, symbols). The spectra are normalized at the maxima. The solid lines give the results of model calculations.

luminescence bands associated with the recombination of electrons and deeply localized holes, whose Bohr radius is smaller than the Thomas-Fermi screening radius $a_B \leqslant q_{TF}^{-1}$, can appear. Here, $q_{TF}=\sqrt{3}\omega_{pl}/v_F$ is the Thomas-Fermi wave vector, ω_{pl} is the frequency of the free-carrier plasmon, and v_F is the velocity of electrons on the Fermi sphere of radius $p_F/\hbar=(3\pi^2 n_e)^{1/3}$ in the reciprocal space. These bands must be redshifted as compared with the band-to-band luminescence, and they can coexist with the Urbach tails of the band-to-band luminescence, as in GaAs and GaN.

We consider a model description of the density of states of the valence bands, taking into account both the Urbach tail and acceptor states of different localization depths. The behavior of the density of states in the Urbach tail is commonly well described in a wide-energy range by the exponential law.[36,37] Taking the density of acceptor states in the Gaussian form, we write the model density of states for holes as

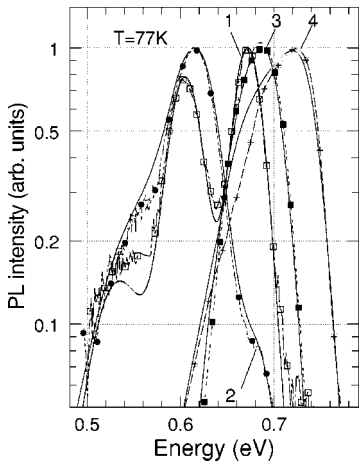

FIG. 11. PL spectra of samples Gs055 and Gs2019 of the second group and samples E233-5 and 000702 of the third group (curves 1, 2, 3, and 4, respectively) at nitrogen temperature. The spectra are normalized at maxima. The symbols are experimental data, and the solid lines give the results of model calculations.

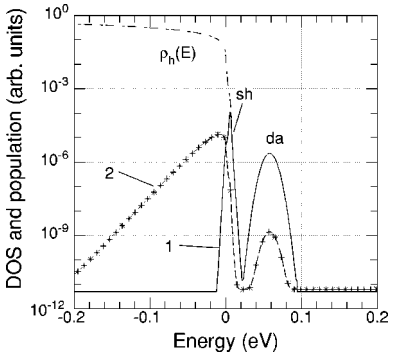

FIG. 12. Model density of the valence-band states $\rho_h(E)$ (dot-and-dashed curve), including the Urbach tail at $E_U^h=1$ meV and acceptor states *sh* and *da*. Curves 1 and 2 are the hole populations at liquid-helium and room temperatures, respectively.

$$\rho^h(E) \sim \left[\frac{(2m_h)^{3/2}v_0}{4\pi^2\hbar^3}\right]\sqrt{|E|}, \tag{1}$$

below the valence-band top, where E is negative and $|E|>E_U^h/2$ and v_0 is the volume of the elementary cell of the lattice. Then, at $E>-E_U^h/2$, the density of the hole states can be represented as

$$\rho^h(E) \sim \left[\frac{(2m_h)^{3/2}v_0}{4\pi^2\hbar^3}\right]\sqrt{E_U^h/2}\,\exp[-(E-E_U^h/2)/E_U^h] + \frac{N_{sh}}{(2\pi\gamma_{sh})^{1/2}}\exp\left\{-\left[\frac{\hbar\omega-E_{sh}}{2\gamma_{sh}}\right]^2\right\} + \frac{N_{da}}{(2\pi\gamma_{da})^{1/2}}\exp\left\{-\left[\frac{\hbar\omega-E_{\mathrm{da}}}{2\gamma_{da}}\right]^2\right\}, \tag{2}$$

where E_U^h is the characteristic Urbach energy determining the typical localization energy and the radius of the bound state ($r_{loc}=\sqrt{[\hbar^2/(2m_hE_U^h)]}$); E_{sh}, γ_{sh}, N_{sh}, E_{da}, γ_{da}, and N_{da} are the localization energies, inhomogeneous broadenings, and dimensionless concentrations of the shallow and deep acceptors, respectively, and m_h is the hole effective mass. The Urbach parameter E_U^h in the calculations was taken to be 1 meV. This model density of states is given in Fig. 12.

B. Different limits of photohole distribution

It can be expected that the concentration of the localized valence-band states in *n*-InN samples now available is still smaller than the electron concentration. If localized states are spread over a wide energy range then, first of all, the dependence on the filling of these states at relatively low excitation powers can influence the PL band.

The steady-state luminescence depends on the distribution of the photoholes over the valence-band states and, hence, their energy-relaxation rate and also on the excitation power.

In the limit of the weak excitation of samples characterized by a powerful tail of localized states and fast relaxation rate, we can expect that only the holes localized by the deepest (spatially isolated from each other) states[19] will define the PL-band shape. The stationary occupancy of these states is not equilibrium because they are isolated, and, at low tem-

peratures, the number of holes at a given localization energy is simply proportional to the density of states. The PL mechanism of this kind was observed in the spectra of disordered systems under weak excitations, when recombining excitons were captured by the localized states of the tail.[38]

The hole distribution in this limit is expected to be nondegenerate, and the temperature increase can lead to the Boltzman distribution of populated states. The influence of the steady-state excitation power must be weak as long as the hole distribution remains nondegenerate.

The "strong" excitation limit can be reached if the number of photoholes created by excitation is comparable to the number of localized states in the tail of the valence band. If in this case the energy relaxation time $\tau_E(T)$ is much less than the full temperature-dependent lifetime $\tau(T)$ of holes in radiative states, a degenerated distribution of the holes can be expected. We denote the generation rate of the photoholes as G. Then the chemical potential of the photoholes $\mu^h(G,T)$ that defines their equilibrium or almost-equilibrium distribution can be found from

$$G\tau(T) = \int_{-\infty}^{\infty} [1 - n_E^h(G,T)]\rho_h(E)dE, \tag{3}$$

where the Fermi-distribution function for the valence band is

$$n_E^h(G,T) = \frac{1}{\exp\{[E - \mu^h(G,T)]/T\} + 1}, \tag{4}$$

and the temperature is expressed in the energy units. Since the $\tau(T)$ is temperature dependent, $\mu^h(G,T)$ must also depend on temperature. At not-too-strong excitations $\mu^h(G,T)$ must be positive and lie above the valence-band top. The hole chemical potential $\mu^h(G,T)$ at increasing excitation power at low temperatures becomes negative, resulting in the valence-band-state population.

The really strong excitation limit will be achieved if the localized hole states are saturated, and the electron concentration noticeably increases. It can be expected that the PL-band profile in the strong excitation limit will be sensitive to the excitation power as well as to the temperature.

In Fig. 12 a redistribution of the photohole population at the temperature rise from 4.2 to 300 K is presented. For simplicity, the position of the hole chemical potential just above the shallow acceptor state was not changed. However, a considerable depopulation of localized states takes place even at these conditions. As a result of similar redistribution the localized states lose their role in the PL formation.

C. Conduction-band states

We present the density of states of the conduction band $\rho^e(E)$ (see Fig. 13) in a form similar to those of Eqs. (1) and (2),

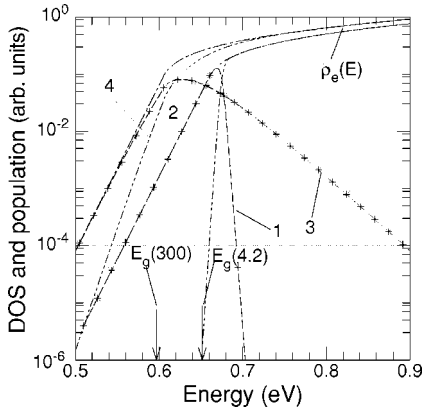

FIG. 13. Model densities of the conduction-band states $\rho_e(E)$ at two temperatures, with the Urbach tail at E_U^e=15 meV. $E_g(4.2)$ and $E_g(300)$ are positions of the band gap at liquid-helium and room temperatures, curves 1 and 3 are the densities of the populated states, and curves 2 and 4 are the densities of the empty electron states at these temperatures, respectively.

$$\rho^e(E) \sim \left[\frac{(2m_e)^{3/2}v_0}{4\pi^2\hbar^3}\right]\sqrt{[E - E_g(n,T)]}, \tag{5}$$

at $[E-E_g(n,T)] > E_U^e/2$ and

$$\rho^e(E) \sim \left[\frac{(2m_e)^{3/2}v_0}{4\pi^2\hbar^3}\right]\sqrt{E_U^e/2} \sim \times \exp\{-[|E - E_g(n,T)| - E_U^e/2]/E_U^e\}, \tag{6}$$

at $[E-E_g(n,T)] < E_U^e/2$, where E_U^e is the characteristic Urbach energy that determines the typical energy of electron localization, and $E_g(n,T)$ is the band gap, depending on the electron concentration and on temperature. The parameter E_U^e for the samples of high quality ranged from 7.5 to 15 meV.

The origin of the localized states that lie below the bottom of the conduction band may be associated with, e.g., spatial fluctuations in the positions of shallow donors. For example, if the Bohr radius of a Coulomb center is $a_B > q_{TF}^{-1}$, then the bound state on a single center will disappear, but a pair of such centers situated within a sphere of radius q_{TF}^{-1} may lead to the formation of a shallow localized state.

The dependence of the band gap $E_g(n,T)$ on the electron concentration, which is due to the Hartri-Fock exchange interaction, is taken in the form,[5]

$$E_g(n,T) = E_g(0,T) - 20(n/10^{18})^{1/3}. \tag{7}$$

Here, $E_g(n,T)$ is the band gap expressed in meV's at electron concentration n expressed in cm^{-3}, and $E_g(0,T)$ is the band gap in the limit of zero electron concentration. A numerical factor was estimated in Ref. 5. We assume that the temperature dependence of the band gap is universal and does not change with electron concentration.

The Fermi energy of the conduction band, $E_F = p_F^2/2m_e$ in meV's, for the parabolic electron band is[5]

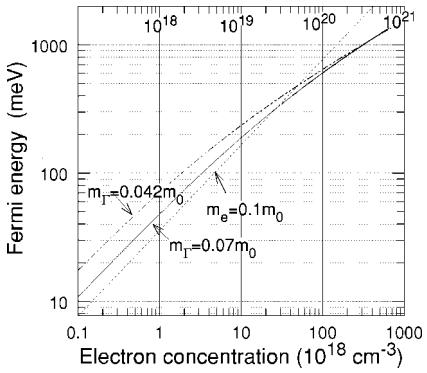

FIG. 14. Model dependences of the Fermi energy on electron concentration for parabolic and nonparabolic dispersions of the conduction band. Dotted line corresponds to the parabolic band with $m_e=0.1m_0$. Dash-and-dot and solid lines correspond to the nonparabolic band with the linear dependence of effective mass on the electron kinetic energy $m_e=m_\Gamma(1+E/E_0)$. The effective masses at the Γ-point are taken to be $0.042m_0$ and $0.07m_0$.

$$E_F = 3.58(m_0/m_e)(n/10^{18})^{2/3}, \tag{8}$$

where m_e is the effective mass of an electron, m_0 is the free-electron mass, and a numerical factor is found for the parabolic band by using the well-known expression for E_F from Ref. 39.

If the effective mass linearly increases[27] with the electron kinetic energy, $[E-E_g(n,T)]$,

$$m_e = m_\Gamma\{1 + [E - E_g(n,T)]/E_0\}, \tag{9}$$

where m_Γ is the electron effective mass at the Γ point, and E_0 is the kinetic energy at which the effective mass doubles, then the Fermi energy dependence on concentration can be described by

$$E_F = E_0\{[(3.58/E_0)(m_0/m_\Gamma)(n/10^{18})^{2/3} + 1/4]^{1/2} - 1/2\}. \tag{10}$$

The Fermi energies as functions of concentration for parabolic and nonparabolic bands are presented in Fig. 14.

It is possible to use the plasmon frequency to estimate the electron concentration, and the corresponding expression for it in the case of the nonparabolic band at zero wave vectors is

$$\omega_{pl}^2 = \frac{4\pi e^2 n_e}{\varepsilon_L(\omega_{pl})m_\Gamma}\left[\frac{k_0}{p_F}\right]^3\left[\frac{p_F}{k_0} - \arctan\left(\frac{p_F}{k_0}\right)\right], \tag{11}$$

where

$$k_0^2 = 4m_\Gamma E_0, \tag{12}$$

and

$$p_F^2 = 2m_\Gamma E_F(1 + E_F/E_0), \tag{13}$$

and $\varepsilon_L(\omega_{pl})$ is the dielectric function taken at $\omega=\omega_{pl}$ and at zero wave vector and including both the lattice and interband susceptibilities. Therefore, Eq. (11) is, in the general case, the equation defining the plasmon frequency for a nonparabolic band.

This equation can be simplified if (p_f/k_0) is low enough and $\arctan(p_f/k_0)$ can be represented as a Taylor power series. This leads to the expression,

$$\omega_{pl}^2 = \frac{4\pi e^2 n_e}{\varepsilon_L(\omega_{pl})m_\Gamma}\left[1 - \frac{3}{5}\left\{\frac{p_F}{k_0}\right\}^2\right]. \tag{14}$$

The conditions

$$a_B \leqslant q_{YF}^{-1}$$

and

$$T \ll E_F = p_F^2/2m_e$$

define the ranges of temperatures and electron concentrations corresponding to the degenerate distribution of electrons in doped crystals.

D. Interband PL and absorption spectra

The interband optical absorption in doped crystals is formed by transitions from populated states of the valence bands to unpopulated states of the conduction band. This results in the Burstein-Moss shift of the optical-absorption edge for the energy of the order of E_F[5].

The high-energy band of the interband photoluminescence arises due to the annihilation of the photoexcited holes and electrons, which are still degenerate in the high-quality samples available now. As a consequence, the PL-band width at low temperatures is determined by E_F. The nonparabolicity of the electron band affects both the absorption-coefficient profile and the luminescence-band shape.

In the samples with the electron concentration $n\approx 1\times 10^{18}$, $E_F\approx 35$ meV for the parabolic band at $m_e=0.1m_0$ or 48 and 71 meV for the nonparabolic one at $m_\Gamma=0.07m_0$ and $0.042m_0$, respectively.

Under this condition, the shallow hole and electron states that form exponentially decaying Urbach tails of the density of states of the valence and conduction bands can play an important role in PL-band shape formation. The luminescence bands formed by the recombination of electrons and deeply localized holes are redshifted, as in the case of GaAs and GaN. However, the tails of the more shallow states typically exist together with the deep states.

1. Absorption

It should be noted that the dopants that are randomly distributed over the crystal and various defects of the crystal lattice affect the motion of electrons and holes. Scattering from a random potential created by impurities and defects breaks the momentum-conservation law. As a consequence, the sum of the electron $\mathbf{p}_e$ and hole $\mathbf{p}_h$ momenta are not equal to the momentum of a photon, which results in nonvertical interband transitions.

Then energies of the electron and hole can be written in the effective-mass approximation as

$$E_e = \frac{(\mathbf{p} + \mathbf{Q}\mu/m_h)^2}{2m_e}, \tag{15}$$

and

$$E_h = -\frac{(\mathbf{p} - \mathbf{Q}\mu/m_e)^2}{2m_h}, \tag{16}$$

respectively, and the energy of a pair created upon the absorption of a photon is

$$\hbar\omega = E_g(n,T) + \frac{p^2}{2\mu} + \frac{Q^2}{2M}. \tag{17}$$

Here, $\mathbf{Q}=(\mathbf{p}_e-\mathbf{p}_h)$ is the center of the mass momentum and $\mathbf{p}=(\mathbf{p}_e\mu/m_e+\mathbf{p}_h\mu/m_h)$ is the momentum of relative motion, where μ and $M=(m_e+m_h)$ are the reduced and translation masses of the pair, respectively. The energy dependence of the band-to-band contribution to the dielectric susceptibility that determines the behavior of the absorption coefficient can be represented as

$$\chi''(\omega) \sim \frac{v_0}{(2\pi\hbar)^3}\int d^3p\, d^3\, Q n^h_{\mathbf{p}}\left[\frac{(\mathbf{p} - \mathbf{Q}\mu/m_e)^2}{2m_h}\right] \times\Delta(\mathbf{Q})\delta\left(\hbar\omega - E_g - \frac{p^2}{2\mu} - \frac{Q^2}{2M}\right) \times\left\{1 - n^e_{\mathbf{p}}\left[\frac{(\mathbf{p} + \mathbf{Q}\mu/m_h)^2}{2m_e}\right]\right\}. \tag{18}$$

Here, v_0 is the elementary cell volume, and $n^e_{\mathbf{p}}$ and $n^h_{\mathbf{p}}$ are the Fermi functions of electrons and holes. The spin quantum numbers are omitted for simplicity.

$\Delta(\mathbf{Q})$ is the squared, overlapping integral between the wave functions of the electron and hole that are created at the same point of space by a photon, and whose momentum of the center of mass is $\mathbf{Q}$,

$$\Delta(\mathbf{Q}) = |\psi^e_{\mathbf{p}+\mathbf{Q}}(\mathbf{r})\psi^h_{\mathbf{p}-\mathbf{Q}}(\mathbf{r})|^2. \tag{19}$$

In the case of the free motion of electrons and holes,

$$\Delta(\mathbf{Q}) \to \delta(\mathbf{Q}), \tag{20}$$

i.e., the function reduces to a three-dimensional (3D) delta function that expresses the momentum-conservation law. In this case only vertical transitions are allowed, and the kinetic energies of the created hole and electron depend only on the ratio of the effective masses,

$$E_h = -(m_e/m_h)E_e. \tag{21}$$

The quantity $\mathbf{Q}$ may take a continuum set of values for different mechanisms of the scattering of electrons and holes from defects, and it is necessary to perform summation over these values. If $\Delta(\mathbf{Q})$ does not restrict the possible values of $\mathbf{Q}$, then the integration with respect to d^3Q extends over the entire volume of the first Brillouin zone. The hole kinetic energy is restricted by the energy-conservation law alone,

$$0 \leqslant E_h \leqslant [\hbar\omega - E_g(n,T)]. \tag{22}$$

Since the population of the valence band in the calculations of the absorption coefficient can be taken as equal to unity, we present the energy dependence of the imaginary part of the interband susceptibility and of the absorption coefficient for parabolic bands in these two limiting cases[5] as

$$\chi''(\omega) \sim \left[\frac{\hbar\omega - E_g(n,T)}{E_g(n,T)}\right]^{\gamma/2}\left\{1 - \frac{1}{\left[\exp\left(\{\frac{\mu}{m_e}[\hbar\omega - E_g(n,T)] - E_F\}/T\right) + 1\right]}\right\}. \tag{23}$$

In the case in which the conservation law is obeyed, $\gamma=1$, whereas in the absence of limitations on the momenta, $\gamma=4$.

In the intermediate case, in which the momentum-conservation law is partially broken, the interpolation formula is

$$\chi''(\omega) \sim \int_{E_g(n,T)}^{\infty}\rho^e(E)dE\int_{-\infty}^{0}dE_1\,\rho^h(E_1)\Phi_{E,E_1} \times\delta[\hbar\omega - E_g(n,T) - E + E_1][1 - n^e_E(T)], \tag{24}$$

where the square of the overlapping integral takes the form,

$$\Phi_{E,E_1} = \left|\int d^3r\,\psi^e_E(\mathbf{r})\psi^h_{E_1}(\mathbf{r})\right|^2, \tag{25}$$

and the wave functions of the electron and hole $\psi^e_E(\mathbf{r})$ and $\psi^h_{E_1}(\mathbf{r})$ are not characterized now by momenta. For an accurate calculation of Eq. (25) we should know these wave functions. An approximate equation can be obtained by replacing Eq. (25) by the Gaussian function that has a maximum when the kinetic energies of particles satisfy Eq. (21), i.e., at $|E_1| = (m_e/m_h)E$. By varying the broadening of this function, we transform the susceptibility dependence in the limits defined by Eq. (23).

For a nonparabolic electron band the susceptibility can also be calculated through Eq. (24). As demonstrated by Carrier and Wei,[27] the nonparabolicity leads to an enhancement in the energy dependence of the absorption coefficient as compared with the parabolic electron band if the momentum-conservation law is fulfilled. Calculations using Eq. (24) show that the susceptibility behavior can be characterized by the index $\gamma\approx 3$ in Eq. (21) if the momentum-conservation law is satisfied. The breaking of the conservation law leads to a further enhancement of the dependence, though the difference between the two limiting cases is not as strong as that for the parabolic band.

The localized states of electrons are filled in materials of the *n* type. Taking into account the localized states of holes, we transform Eqs. (24) and (25) into

$$\chi''(\omega) \sim \int_0^{\infty} \rho^e(E)dE \int_{E_g(n,T)}^{-\infty} dE_1\, \rho^h(E_1)\Phi_{E,E_1} \times \delta[\hbar\omega - E_g(n,T) - E + E_1] n^h_{E_1}(G,T) \times [1 - n^e_E(T)], \tag{26}$$

where now

$$\Phi_{E,E_1} = \left| \sum_{\lambda} \int d^3r\, \psi^e_E(\mathbf{r}) \psi^h_{E_\lambda = E_1}(\mathbf{r}) \right|^2. \tag{27}$$

Here, $\psi^h_{E_\lambda = E_1}(\mathbf{r})$ is the wave function of the hole, λ is a complete set of quantum numbers of the state, and the eigenvalues of the state E_λ are E_1. The heavy-hole states usually dominate in the interband absorption. The acceptor states of the heavy hole only slightly restrict the possible set of electron states participating in transitions, because of a large difference in the effective masses of the electron and the heavy hole assumed for InN. The wave vectors of electrons allowed in this process are of the order of $p_e \leqslant (2m_h E_1/\hbar^2)^{1/2}$. The restrictions on band-to-band transitions remain the same.

The electron-hole pair created by a photon is electrically neutral. The inhomogeneous distribution of dopants results in spatial fluctuations of the potential energies of an electron and hole. The changes in the potential energies of an electron and hole in the field of an inhomogeneously distributed electrical charge have opposite signs and do not alter the band gap, but do modify the degenerate-electron-density distribution, which becomes nonuniform; $n^e_E \rightarrow n^e_E[E - \phi(\mathbf{r})]$, i.e., the distribution becomes dependent on the potential energy $\phi(\mathbf{r})$,

$$n^e_E[E - \phi(\mathbf{r})] = \frac{1}{\exp\{[E - \phi(\mathbf{r}) - \mu^e]/T\} + 1}, \tag{28}$$

where μ^e is the chemical potential of the electron band. Direct measurements have shown that a considerable band bending of InN samples takes place.[28–32] According to Ref. 32, the carrier concentration decreases roughly as the square root of the sample thickness.

The absorption coefficient for an inhomogeneous sample can be written in terms of the averaged contribution of interband transitions to the dielectric susceptibility,

$$\langle \chi''(\omega) \rangle = \langle \chi''(\omega, \phi) \rangle_\phi, \tag{29}$$

where $\chi''(\omega, \phi)$ is obtained from Eq. (26) by substituting $n^e_E[E - \phi(\mathbf{r})]$ for n^e_E, and the angular brackets denote averaging over the distribution of the values of ϕ. It was shown in Refs. 5 and 19 that an inhomogeneity of the samples produced by charge fluctuation influences the slopes of the high-energy wing of the PL band and the absorption threshold.

2. Photoluminescence

Considering recombination, it is necessary to take into account, in addition to the factors that influence the absorption processes, the additional factors, i.e., the distribution of photoholes and the electron-phonon interaction. The luminescence intensity produced by electron-hole recombination can be represented as

$$I_{PL}(\omega) \sim \int_0^{\infty} \rho^e(E)dE \int_{E_g(n,T)}^{-\infty} dE_1\, \rho^h(E_1)\Phi_{E,E_1} \times \delta[\hbar\omega - E_g(n,T) - E + E_1] \times [1 - n^h_{E_1}(G,T)] n^e_E(T). \tag{30}$$

Here,

$$\Phi_{E,E_1} = \left| \sum_{\lambda,\lambda_1} \int d^3r\, \psi^e_{E_\lambda = E}(\mathbf{r}) \psi^h_{E_{\lambda_1} = E_1}(\mathbf{r}) \right|^2 \tag{31}$$

is the overlapping integral between the electron and hole wave functions, including the localized acceptor states.

We can assume that the most effective electron-phonon interaction is realized in InN for the deeply localized states, as in other semiconductors. In the spectra of the InN samples studied the recombination of the deep acceptor states is the most probable candidate for observing this effect. As shown in Ref. 15, the first stage of the energy relaxation of photoexcited carriers is very fast and can be attributed to the carrier interaction with longitudinal optical phonons. This feature is shared by many other crystals. Therefore, we can expect an LO-phonon replica of the recombination band of the deep acceptor. This effect can be simulated as an additional band in $\rho^h(E_1)$ proportional to the electron-phonon interaction constant.

IV. RESULTS OF CALCULATIONS AND DISCUSSION

The calculations of the PL spectra were performed for a number of samples of different thicknesses having different electron concentrations estimated by conventional Hall measurements. The major goal of the calculations was to establish the origin of the PL and the InN fundamental parameters that would be appropriate for the description of the experimental data on photoluminescence and absorption.

The variable parameters were the band gap $E_g(n,T)$ at $n=0$ and $T=0$, the electron effective mass at the Γ point, the free-carrier concentration, the band-gap shrinkage from liquid-helium to room temperatures, and the binding energies of shallow and deep acceptors.

In our analysis, the band gap $E_g(0,0)$ was varied from 0.665 to 0.675 eV. These values allowed us to describe the PL and absorption experimental data using the band-gap dependence on the electron concentration given by Eq. (10). However, further calculations showed that the band-gap value must be matched with the band-gap shrinkage and the binding energies of the acceptors. The band-gap-temperature shrinkage from liquid-helium to room temperatures had to be taken in the limits 55–65 meV, depending on the band gap

chosen. The acceptor binding energies of the model also depended on the band gap and were lying in the range of 50–60 meV for deep acceptors and 5–15 meV for shallow ones. The ratio between the effective masses of electron and hole m_Γ/m_h was taken to be 1:10.

A simultaneous fitting of the PL, absorption, and band-gap shrinkage leads to the conclusion that the band gap $E_g(0,0)$ should be taken to be equal or less than 0.670 eV; otherwise the temperature shrinkage should be taken larger than 60 meV, i.e., too close to the value for the wide-gap GaN crystal (see, for instance, Ref. 40).

If the band-gap values are chosen to be within the interval 0.665–0.670 eV, then the band-gap shrinkage between liquid-helium and room temperatures should be restricted by 55–60 meV, and the energies of 50–55 and 5–10 meV for deep and shallow acceptors, respectively, are sufficient to describe the PL spectra. In this case the role of the shallow acceptors can be attributed to the Urbach tail of the valence band with the appropriate E_U^h. An analysis of the PL and absorption spectra shows that the band gap at room temperature is about 0.6 eV.

The model parameters used in the calculations, including the nonparabolic effective mass, are summarized in Figs. 12–14.

The band gaps of 0.690 eV or 0.692 eV suggested in Refs. 13–18 seem to be too wide, because these values can hardly be reconciled with the relatively small band-gap shrinkage observed in Ref. 13.

The electron effective mass at the Γ point equal to $0.07m_0$ as suggested in Ref. 27 (or the value $0.085m_0$ from Ref. 9) can be considered as a best choice, though it leads to electron concentrations differing from the Hall data (see Table I).

The Hall concentrations give at these conditions Fermi energies that are too high and do not correspond to the observed PL-band widths. Despite data[28–32] allowing one to assume a high-enough inhomogeneity in the surface or interface layers, it looks reasonable to restrict the minimal concentrations in the high-quality samples from below by the values on the order of $1-2\times10^{17}$ cm^{-3}.

At this restriction, the value $m_\Gamma=0.042m_0$ (Ref. 18) is acceptable to fit the PL-band shapes, though it leads to noticeably stronger deviations of optical electron concentrations from the conventional Hall values than the larger m_Γ.

A. Structure of the PL spectra

The PL spectra of the samples of the first and second groups demonstrate the structure characterized by three stable features: the high-energy peak I_{sh}, the middle-energy peak I_{da}, and the weak low-energy peak I_{da}-LO (Figs. 1–3 and 5–9). The high-energy peak is attributed to the overlapping bands produced by two mechanisms, namely, by the transitions of the degenerate electrons to shallow acceptor and/or Urbach tail states and by band-to-band transitions.

In Ref. 18 a similar feature of the PL spectrum for the sample with Hall concentration 7.7×10^{17} cm^{-3} is attributed to the transitions of nondegenerate electrons from the bottom of the conduction band to the states of shallow acceptors. However, the assumption that the electrons are nondegenerate seems to contradict the Hall data.

The second peak is likely to be attributable to the electron transitions to the deep-acceptor states, as suggested in Ref. 18.

The third feature is about 73 meV below the electron deep-acceptor transitions. This energy coincides with the LO-phonon energy, according to the Raman data.[35] To describe the third feature of the PL spectra, it is necessary to assume that the dimensionless electron-phonon constant is ≈0.02, which corresponds to a weak electron-phonon interaction. This value was found to be nearly independent of the carrier concentration.

The PL structure becomes less pronounced with decreasing sample thickness (accompanied by the concentration increase) and disappears from the spectra of the samples with the Hall concentrations above 10^{18} cm^{-3}.

B. Temperature dependence of the PL and absorption spectra

The PL spectra of the samples of the first and second groups exhibit a strong variability in the range between liquid-helium and nitrogen temperatures at a constant excitation power (Figs. 1, 3, 6, and 8). The sensitivity of the PL spectrum to the temperature shows that the population of one of two types of carriers forming the PL band is strongly influenced by temperature. On the other hand, the Hall data give evidence that the electrons are still degenerate. Then, the relative decrease in the high-energy peak with temperature can be assigned to the redistribution of the population between the shallow and deep localized states of holes.

Therefore, we can assume that the energy relaxation of photoholes is fast enough, so that it is possible to consider the hole distribution as equilibrium or almost equilibrium.

The spectra transformations cannot be ascribed to the simple thermal redistribution of holes between deep and shallow acceptors at a constant chemical potential of holes. However, they can be produced by a simultaneous shift of $\mu^h(G,T)$ toward the band gap. According to Eq. (3), this fact shows that the full relaxation time of holes $\tau(T)$ decreases with increasing temperature. For the high-quality samples, at liquid-helium temperature and at the highest excitation power applied, $\mu^h(G,T)$ is several meV's above the shallow-acceptor level.

The PL-band shapes are influenced by the inhomogeneous distribution of electrons. This results in a difference between the observed slope of the high-energy wing of the PL band in the low-temperature spectra and the slope that would follow from the Fermi function at a given temperature. Therefore, the observed slope at the liquid-helium temperature in the spectra of the high-quality samples corresponds to an effective temperature equal to about 15 K. As a result, the effective temperature can be introduced instead of the more complex averaging procedure of Eq. (29). The difference between the real and effective temperatures increases for the samples of the third group. This can be

attributed to the inhomogeneous distribution of the charge density.[28–32]

The PL spectra experience transformations when the samples are heated to room temperature. A considerable shift and broadening of the PL band is accompanied by a disappearance of the structure. The model calculations show that the temperature increase causes considerable broadenings of the electron and hole distributions (Figs. 12 and 13). In the high-quality samples, this results in a partial removal of the electron degeneration (see Fig. 13). The thermal band-gap shrinkage shifts the PL band to low energies, while an increase in the kinetic energies of carriers produces effects of the opposite sign. As a result of these two tendencies, the observed shift of the PL band can take different values for samples of different qualities.

The microscopic mechanism regulating the temperature behavior of the PL-band shift is formed, on the one hand, by the difference in masses of the electron and heavy hole and, hence, by the different values of their thermal momenta, $p_T^h = \sqrt{2m_h T}$ and $p_T^e = \sqrt{2m_e T}$, respectively. On the other hand, under these conditions, an important question arises as to whether the momentum-conservation law is obeyed in the annihilation processes or not. Depending on this, the interband transitions between states with different momenta can be allowed or restricted.

For instance, the PL-band profiles of *p*-type samples of GaAs and GaSb are strongly influenced by the restriction following from the momentum-conservation law, as demonstrated by Titkov *et al.*[41] As a result, transitions involving hole states with large momenta are suppressed.

An analogous restriction arises in samples of *n*-type InN if their quality is high enough. High thermal momenta of holes p_T^h corresponding to the maximum of their thermal distributions prevent their annihilation with electrons whose momenta are of the order of p_F or p_T^e. In this case transitions of electron to the valence-band states with $p^h \approx p^e$ occur, and the PL-band position is affected, as temperature increases, by band-gap shrinkage and also by the high-energy shift of the electron distribution. On the other hand, breaking of the law involves the thermal holes in recombination and additionally increases the PL-band energy by $\approx$30 meV. The interplay of different factors influencing the PL-band position leads to a variability of the PL-band shift with temperature.

The other circumstance worth noting is the dependence of the PL-band maximum on the violation of the momentum conservation at a large difference between the electron and the heavy hole masses even at constant temperature. As a result, it can be expected that the PL band of the sample containing a higher concentration of scatterers will be shifted towards higher energies at equal carrier concentrations and temperatures.

Simultaneous fits of PL and absorption spectra at liquid-helium, nitrogen, and room temperatures are presented in Figs. 3(a)–3(c). The question arises as to whether it is possible to find the band gap or the band-gap shrinkage directly from the spectra. Note that the nonparabolicity of the conduction band, the influence of the band-filling effect, the nonuniform carrier density, and the breaking of the momentum-conservation law in optical transitions make impossible the use of the simple $\alpha^2(E)$ extrapolation for finding the band-gap and the band gap shrinkage.

An attractive idea to use the sigmoidal equation[13,42] to describe the spectral dependence of the absorption is also unsuited for the accurate estimation of these characteristics. As a matter of fact, the absorption spectra of thick samples, similar to those presented in Figs. 3(a)–3(c), demonstrate a point at which the Bregg interference disappears, which seems to be closer to the band gap than other possible characteristics of the spectra.

An interesting feature of the room-temperature luminescence is the disappearance of any structure associated with acceptor and phonon replicas. This can be interpreted as a result of a large difference between the densities of localized and band-hole states. Figure 4 demonstrates the results of model calculations of the PL-band profile with and without acceptor states (curves 1 and 3, respectively). Therefore, at room temperature the major part of the photoholes occupies the valence-band states, and the luminescence produced by the localized hole states is too weak to be identified.

C. Dependence of the PL spectra on the excitation power

Figures 2, 7, and 9 demonstrate the dependences of the PL spectra on the excitation power at nitrogen temperature for the samples of the first and second groups. Qualitatively, the changes in the spectra with decreasing excitation power are similar to those occurring at rising temperature. The details of the dependences can be understood by taking into account the correlations between the number of electron-hole pairs excited by photons and, on the one hand, the number of localized hole states and, on the other hand, the number of free electrons.

If the excited-pair concentration is comparable with concentration of localized hole states, but less than the electron concentration, then the behavior of the PL spectra can be understood in terms of a shift of the hole chemical potential [see Eq. (3)] due to the generation-rate alterations. It is worth noting that in the samples of high quality at relatively low excitations only the magnitude redistribution between two high-energy maxima is observed, without any pronounced shifts of the high-energy PL-band maximum. This can be interpreted as a manifestation of the population redistribution between the deep and shallow localized states of holes.

If the excitation power is enhanced up to a level at which the created electron-hole-pair concentration becomes comparable with the free-carrier concentration, then the broadening and the shift of the spectra can be observed as it is demonstrated in Fig. 2.

An excitation-induced increase of electron concentrations from 2.4×10^{17} at a low-excitation level to 4.2×10^{17} cm^{-3} at the maximum-pulse excitation is established for sample Gs2060 (see Fig. 2).

The PL spectrum of sample E233-5 with the Hall concentration 1.7×10^{18} cm^{-3} given in Fig. 10 can be seen to exhibit another behavior. Only a small, high-energy shift of the PL band with increasing excitation power is observed. The increase in the energy of the PL-band maximum points to a continuum spectrum of acceptor states, rather than a discrete

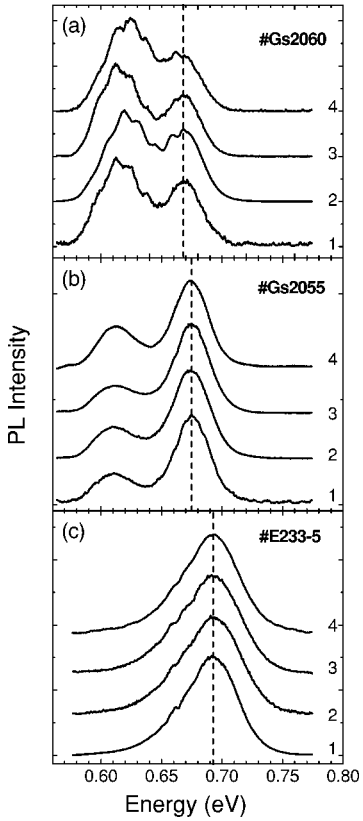

FIG. 15. PL spectra of samples Gs2060, Gs2055, and E-233-5 at different excitation energies. Curves 1, 2, 3, and 4 were obtained with excitation energies 2.33, 1.55, 1.10, and 0.81 eV, respectively. The spectra were detected with a InGaAs-detector.

one, and it can be explained by the shift of the hole chemical potential toward the valence-band top and the simultaneous increase of the electron concentration. A strong influence of the excitation power on the electron concentration was described in Ref. 16 for a sample with the Hall concentration 1.3×10^{18} cm^{-3}.

The measurements of the PL spectra were performed for all set of the samples using the lasers operating in the energy range from 2.41 eV to 0.81 eV as excitation sources. Our results show that the PL-spectra shapes are affected by excitation density, rather than by excitation energy. For all excitation energies, the changes in excitation density result in the redistribution of PL intensity between the band-edge-related peak and the impurity-related peak for samples of the first and second groups. No changes were observed for the PL-band shape of the samples of the third group. These findings are typical of all direct-band-gap semiconductors. As an example, Fig. 15 shows the luminescence spectra of three InN samples with different carrier concentrations obtained at four laser energies. Each laser was adjusted to keep approximately the same excitation density (about 50 wt. %/cm^2). This excitation level corresponds to curve 2 on Fig. 2 for the sample Gs2060.

D. Dependence of the PL spectra on the carrier concentration

For the samples of the first group, the difference in the concentrations obtained from the optical and the Hall data increases as the sample thickness decreases. Nevertheless, the PL spectra of the samples of this group at low excitation levels can be described at the same electron concentration (Fig. 5 and Table I) under the assumption that there is a small difference in the chemical potentials of holes.

The features of the PL spectra of two samples of the second group are similar to those of the samples of the first group [Figs. 6–9 and in Fig. 11 (curves 1 and 2)]. The optical data of these samples give increased electron concentrations as compared with the samples of the first group. For the samples of the third group, the PL-spectrum structure is absent (see Fig. 10 and curves 3 and 4 in Fig. 11).

The electron concentrations derived from the PL data at low excitations are always lower than the Hall concentrations. Taking into account the inhomogeneous distribution of the electron density in InN samples,[28–32] we can conclude that the PL formation occurs in relatively deep layers where the concentration is lower than the averaged value given by the Hall experiments. Probably, the surface layer is characterized by the hole lifetime, which is small enough as compared with the radiative recombination time and is insufficient to form photoluminescence. The data on the mobility decrease in near-surface layers[28–32] indirectly support this idea.

V. CONCLUSIONS

The interband photoluminescence and absorption spectra of *n*-InN samples with electron concentrations from 3.6×10^{17} to 6×10^{18} cm^{-3} have been studied. The sample thicknesses were in the range from 12 to 0.47 μm. The well-resolved structure consisting of three peaks in the energy interval from 0.50 to 0.67 eV was observed in the high-quality samples at liquid-helium and nitrogen temperatures. We attribute two lower-energy PL peaks to the recombination of degenerate electrons with the holes trapped by deep acceptors and to the LO-phonon replica of this band. The higher-energy PL peak is considered to be a complex band formed by transitions of electrons to the states of shallow acceptors and/or the states of the Urbach tail populated by photoholes and also by the band-to-band recombination of free holes and electrons.

The strong dependences of the intensities of the two higher-energy PL peaks on the excitation power and temperature have been found. The model approach that takes into account the Urbach tails of the conduction and valence bands and the acceptor states has been developed. The conduction band was assumed to be nonparabolic. The calculations of the PL and absorption spectra have shown that the band gap of InN in the limit of zero temperature and zero electron concentration is close to 0.665–0.670 eV, and the band-gap shrinkage from zero to room temperature $[E_g(0)-E_g(300)]$ is 55–60 meV. The effective mass of an electron at the Γ point was assumed to be about 0.07 of the free-electron mass. The analysis of the optical data with electron mass $m_\Gamma=0.042m_0$ leads to electron concentrations that are much lower than those obtained from Hall measurements, especially for the high quality samples.

ACKNOWLEDGMENTS

The authors would like to express their gratitude to Professor A. Yoshikawa and Professor A. Yamamoto for supplying the InN samples for our studies and Professor S. H. Wei for providing us with his theoretical results prior to publication. We are thankful to Dr. M. A. Yagowkina and Dr. A. N. Smirnov for their assistance in x-ray and Raman measurements, Dr. N. A. Pikhtin for giving us an opportunity to use his semiconductor lasers, and to Professor A. Titkov, Professor A. Reznitsky, and Professor S. Permogorov for fruitful discussions. This work was partly supported by RFBR (Project Nos. 03-02-17562 and 03-02-17565) and by the Programs "Physics of Solid State Nanostructures," "Low-dimensional quantum structures," and "New materials and structures."

[1] V. A. Tyagaï, A. M. Evstigneev, A. N. Krasiko, A. F. Andreeva, and V. Ya. Malakhov, Fiz. Tekh. Poluprovodn. (S.-Peterburg) **11**, 2142 (1977) [Sov. Phys. Semicond. **11**, 1257 (1977)].
[2] T. L. Tansley and C. P. Foley, J. Appl. Phys. **59**, 3941 (1986).
[3] V. Yu. Davydov, A. A. Klochikhin, R. P. Seisyan, V. V. Emtsev, S. V. Ivanov, F. Bechstedt, J. Furthmüller, H. Harima, A. V. Mudryi, J. Aderhold, O. Semchinova, and J. Graul, Phys. Status Solidi B **229**, R1 (2002).
[4] V. Yu. Davydov, A. A. Klochikhin, V. V. Emtsev, S. V. Ivanov, V. V. Vekshin, F. Bechstedt, J. Furthmüller, H. Harima, A. V. Mudryi, A. Hashimoto, A. Yamamoto, J. Aderhold, J. Graul, and E. E. Haller, Phys. Status Solidi B **230**, R4 (2002).
[5] V. Yu. Davydov, A. A. Klochikhin, V. V. Emtsev, D. A. Kudyukov, S. V. Ivanov, V. V. Vekshin, F. Bechstedt, J. Furthmüller, J. Aderhold, J. Graul, A. V. Mudryi, H. Harima, A. Hashimoto, A. Yamamoto, and E. E. Haller, Phys. Status Solidi B **234**, 787 (2002).
[6] J. Wu, W. Walukiewicz, K. M. Yu, J. W. Ager III, E. E. Haller, H. Lu, W. J. Schaff, Y. Saito, and Y. Nanishi, Appl. Phys. Lett. **80**, 3967 (2002).
[7] J. Wu, W. Walukiewicz, W. Shan, K. M. Yu, J. W. Ager III, E. E. Haller, H. Lu, and W. J. Schaff, Phys. Rev. B **66**, 201403 (2002).
[8] Y. Nanishi, Y. Saito, and T. Yamaguchi, Jpn. J. Appl. Phys., Part 1 **42**, 2549 (2003).
[9] T. Inushima, M. Higashiwaki, and T. Matsui, Phys. Rev. B **68**, 235204 (2003).
[10] E. Burstein, Phys. Rev. **93**, 632 (1954).
[11] H. Lu, W. J. Schaff, J. Hwang, H. Wu, G. Koley, and L. F. Eastman, Appl. Phys. Lett. **79**, 1489 (2001).
[12] H. Lu, W. J. Schaff, L. F. Eastman, J. Wu, W. Walukiewicz, K. M. Yu, J. W. Auger III, E. E. Haller, and O. Ambacher, Conference Digest the 44th Electronic Materials Conference, Santa Barbara CA, 2002 (unpublished).
[13] J. Wu, W. Walukiewicz, W. Shan, K. M. Yu, J. W. Ager III, S. X. Li, E. E. Haller, H. Lu, and W. J. Schaff, J. Appl. Phys. **94**, 4457 (2003).
[14] J. Wu, W. Walukiewicz, S. X. Li, R. Armitage, J. C. Ho, E. R. Weber, E. E. Haller, H. Lu, W. J. Schaff, A. Barcz, and R. Jakiela, Appl. Phys. Lett. **84**, 2805 (2004).
[15] F. Chen, A. N. Cartwright, H. Lu, and W. J. Schaff, Appl. Phys. Lett. **83**, 4984 (2003).
[16] F. Chen, A. N. Cartwright, H. Lu, and W. J. Schaff, Physica E (Amsterdam) **20**, 308 (2004).
[17] F. Chen, A. N. Cartwright, H. Lu, and W. J. Schaff, J. Cryst. Growth **269**, 10 (2004).
[18] B. Arnaudov, T. Paskova, P. P. Paskov, B. Magnusson, E. Valcheva, B. Monemar, H. Lu, W. J. Schaff, H. Amano, and I. Akasaki, Phys. Rev. B **69**, 115216 (2004).
[19] V. Yu. Davydov and A. A. Klochikhin, Semiconductors **38**, 861 (2004) [Fiz. Tekh. Poluprovodn. (S.-Peterburg) **38**, 897 (2004)], (and references therein).
[20] F. Bechstedt, J. Furthmüller, M. Ferhat, L. K. Teles, L. M. R. Scolfaro, J. R. Leite, V. Yu. Davydov, O. Ambacher, and R. Goldhahn, Phys. Status Solidi A **195**, 628 (2003).
[21] S.-H. Wei, X. Nie, I. G. Batyrev, and S. B. Zhang, Phys. Rev. B **67**, 165209 (2003).
[22] M. Usuda, N. Hamada, K. Shiraishi, and A. Oshiyama, Jpn. J. Appl. Phys., Part 1 **43**, L407 (2004).
[23] D. Fritsch, H. Schmidt, and M. Grundmann, Phys. Rev. B **69**, 165204 (2004).
[24] R. Goldhahn, Acta Phys. Pol. A **104**, 123 (2003).
[25] R. Goldhahn, S. Shokhovets, V. Cimalla, L. Spiess, G. Ecke, O. Ambacher, J. Furthmüller, F. Bechstedt, H. Lu, and W. J. Schaff, Mater. Res. Soc. Symp. Proc. **743**, L5.9.1 (2003).
[26] A. Kasic, E. Valcheva, B. Monemar, H. Lu, and W. J. Schaff, Phys. Rev. B **70**, 115217 (2004).
[27] P. Carrier and S.-H. Wei, J. Appl. Phys. **97**, 033707 (2005).
[28] H. Lu, W. J. Schaff, L. F. Eastman, and C. E. Stutz, Appl. Phys. Lett. **82**, 1736 (2003).
[29] I. Mahboob, T. D. Veal, C. F. McConville, H. Lu, and W. J. Schaff, Phys. Rev. Lett. **92**, 036804 (2004).
[30] L. F. J. Piper, T. D. Veal, I. Mahboob, C. F. McConville, H. Lu, and W. J. Schaff, Phys. Rev. B **70**, 115333 (2004).
[31] W. J. Schaff, H. Lu, L. F. Eastman, W. Walukiewicz, K. M. Yu, S. Keller, S. Kurtz, B. Keyes, and L. Gevilas, Electrochemical Society Proceedings, Vol. 2004–6, Honolulu, October 2004, pp. 358–371 .
[32] C. H. Swartz, R. P. Tompkins, N. C. Giles, T. H. Myers, H. Lu, W. J. Schaff, and L. F. Eastman, J. Cryst. Growth **269**, 29 (2004).
[33] K. Xu and A. Yoshikawa, Appl. Phys. Lett. **83**, 251 (2003).
[34] A. G. Bhuiyan, A. Hashimoto, and A. Yamamoto, J. Appl. Phys. **94**, 2779 (2003).
[35] V. Yu. Davydov, V. V. Emtsev, I. N. Goncharuk, A. N. Smirnov, V. D. Petrikov, V. V. Mamutin, V. A. Vekshin, S. V. Ivanov, M. B. Smirnov, and T. Inushima, Appl. Phys. Lett. **75**, 3297 (1999).
[36] A. A. Klochikhin and S. G. Ogloblin, Phys. Rev. B **48**, 3100 (1993).
[37] A. A. Klochikhin, Phys. Rev. B **52**, 10979 (1995).
[38] A. Klochikhin, A. Reznitsky, S. Permogorov, T. Breitkopf, M. Grun, M. Hetterich, C. Klingshirn, V. Lyssenko, W. Langbein, and J. M. Hvam, Phys. Rev. B **59**, 12947 (1999).
[39] D. Pines and P. Nozieres, *The Theory of Quantum Liquids*

(Benjamin, New York, 1966).
[40] I. Vurgaftman, J. R. Meyer, and L. R. Ram-Mohan, J. Appl. Phys. **89**, 5815 (2001).
[41] A. N. Titkov, E. I. Chaikina, E. M. Komova, and N. G. Ermakova, Surf. Sci. **15**, 198 (1981) [Fiz. Tekh. Poluprovodn. (S.-Peterburg) **15**, 345 (1981)].
[42] F. B. Naranjo, M. A. Sánchez-García, F. Calle, E. Calleja, B. Jenichen, and K. H. Ploog, Appl. Phys. Lett. **80**, 231 (2002).